Semaphorin7A patterns neural circuitry in the lateral line of the zebrafish

Agnik Dasgupta[1,*], Sang P. Paik[1,2], Lauren M. Snow[1,3], and A. J. Hudspeth[1,*]

[1] Howard Hughes Medical Institute and Laboratory of Sensory Neuroscience, The Rockefeller University, New York, NY, USA

*Corresponding author: Dr. Agnik Dasgupta
Laboratory of Sensory Neuroscience
The Rockefeller University
New York, NY 10065
Telephone: 212-327-7353
E-mail: adasgupta@rockefeller.edu

[2] Present address: Department of Functional Neuroanatomy, Institute for Anatomy and Cell Biology, Heidelberg University, Heidelberg, Germany

[3] Present address: Brigham and Women's Hospital, Boston, MA, USA

Abstract

In a developing nervous system, axonal arbors often undergo complex rearrangements before neural circuits attain their final innervation topology. In the lateral line sensory system of the zebrafish, developing sensory axons reorganize their terminal arborization patterns to establish precise neural microcircuits around the mechanosensory hair cells. However, a quantitative understanding of the changes in the sensory arbor morphology and the regulators behind the microcircuit assembly remain enigmatic. Here, we report that Semaphorin7A (Sema7A) acts as an important mediator of these processes. Utilizing a semi-automated three-dimensional neurite tracing methodology and computational techniques, we have quantitatively analyzed the morphology of the sensory arbors in wild-type and Sema7A loss-of-function mutants. In contrast to those of wild-type animals, the sensory axons in Sema7A mutants display aberrant arborizations with diminished contacts to hair cells. Moreover, ectopic expression of a secreted form of Sema7A by non-hair cells induces chemotropic guidance of sensory axons. Our findings demonstrate that Sema7A functions both as a juxtracrine and as a secreted cue to pattern neural circuitry during sensory organ development.

Introduction

Pathfinding axons are directed to their appropriate synaptic targets by a variety of guidance cues. While approaching or traversing the target field, the growth cones of migrating axons encounter secreted or cell surface-attached ligands and respond by steering toward or away from their sources (1–4). Fine-grained control of these factors is critical for the establishment of proper neural circuitry.

The zebrafish's lateral line provides a tractable *in vivo* system for exploring the mechanisms that guide the assembly of neural circuits in a peripheral nervous system. In particular, it is possible to detect individual hair cells and the sensory axons that innervate them throughout the first week of development (5). The primary posterior lateral line on each side of the zebrafish's tail consists of about seven neuromasts, which contain mechanoreceptive hair cells of opposing polarities—half sensitive to headward (rostrad) water motion and the

complementary half to tailward (caudad) water motion—that cluster at their centers (6). The sensory axons of the lateral-line nerve branch, arborize, and consolidate around the basolateral surfaces of the hair cells (Fig. 1A). To aid in an animal's swimming behavior, these hair cells sense water currents and relay signals to the brain through the sensory axons (7). The well-defined structure of the ramifications and synaptic contacts of the sensory axons highlight the need to determine the molecular signals behind the assembly of such precise microcircuits (8).

We adopted a candidate-gene strategy to seek factors that direct the growth of afferent growth cones in the zebrafish's lateral line. Analysis of a single-cell RNA sequencing data identified the *semaphorin7a* (*sema7a*) gene to be highly expressed in hair cells of that organ (9). Semaphorins are important regulators of axonal growth and target finding during the patterning of diverse nervous systems (10). The semaphorin family includes proteins that are secreted, transmembrane, and cell surface-attached (11). Among these, Semaphorin7A (Sema7A) is the only molecule that is anchored to the outer leaflet of the lipid bilayer of the cell membrane by a glycosylphosphatidylinositol (GPI) linker (11). Unlike many other semaphorins, which act as repulsive cues (12,13), Sema7A is involved in promoting axon growth (4) and imparting directional signals by interacting with the integrin and plexin families of receptors residing on the pathfinding axons (14–16). Sema7A likely occurs *in vivo* in both GPI-anchored and soluble forms (17–19), and studies of neuronal explants confirm that both forms can induce directed axonal outgrowth (4). Furthermore, it has been proposed that the GPI anchor is cleaved by membrane-resident GPI-specific phospholipases (GPI-PLs) or matrix metalloproteases to release the Sema7A into the extracellular environment and thus regulate dynamic cellular processes (20,21). Because these observations indicate that Sema7A might influence neuronal development both as a juxtracrine and as a diffusive signal, we investigated the role of Sema7A in sculpting a vertebrate peripheral sensory organ.

Results

Sema7A expression and localization in hair cells. The zebrafish genome contains a single *sema7a* gene that produces two transcripts. One transcript encodes Sema7A-GPI, a full-

70 length, GPI-linked, cell surface-attached protein. The second transcript yields Sema7A^{sec}, a
71 protein with a truncated C-terminus, which we conjecture is secreted into the local environment.
72 Each transcript encodes an N-terminal signal sequence and a single copy of the conserved
73 sema domain (11). Using primers that flank the regions encoding the sema domain and the
74 distinct C-termini of the two transcripts, we performed reverse transcription and polymerase
75 chain reactions (RT-PCR) to identify both the membrane-anchored and the secreted transcript
76 in developing larvae (Fig. 1B; Fig. S1A). Single-cell RNA sequencing data also have shown
77 that the *sema7a* transcript is particularly enriched in the immature and mature hair cells of the
78 neuromast during early larval development (9), a period when sensory axons of the posterior
79 lateral line contact hair cells and form synapses with them (5,22). Indeed, we have observed
80 Sema7A to be specifically localized in both mature and immature hair cells (Fig. 1C;
81 Fig. S1B-E).

82 As neuromasts mature, the contacts between sensory axons and hair cells increase in
83 number, become stabilized, and establish synapses (5,22). Because Sema7A can modulate
84 axon guidance (4,14) and synapse formation (15), we wondered whether the level of Sema7A
85 also changes during neuromast development. Upon quantifying the average intensity of
86 Sema7A, we found similar expression in rostrally and caudally polarized hair cells of
87 neuromasts at 1.5, 2, 3, and 4 days post fertilization (dpf). The average Sema7A intensity
88 increased significantly over this period in both rostrally and caudally polarized hair cells. At
89 1.5 dpf, the neuromasts harbor primarily immature hair cells that make minimal contacts with
90 sensory axons and do not form stable association with axonal terminals (22). At this stage the
91 average Sema7A intensity in hair cells remained low. By 2-4 dpf the hair cells mature to form
92 stable contacts and well-defined synapses with the sensory axons (5,23). The average
93 Sema7A intensity in hair cells at each of these stages rose to levels that significantly exceeded
94 those of 1.5 dpf neuromasts (Fig. 1D). This rise in the amount of Sema7A during neuromast
95 maturation supports a role for Sema7A in the guidance of sensory axons and their interaction
96 with hair cells.

97 We additionally demonstrated an anisotropic distribution of Sema7A along the
98 apicobasal axis of each hair cell. As neuromasts develop through 2, 3, and 4 dpf, Sema7A
99 remained highly enriched in the subapical region of the hair cell, the site of the Golgi network.
100 This localization suggests that Sema7A—like other proteins of the semaphorin family (24)—is
101 directed to the plasmalemma through Golgi-mediated vesicular trafficking. While Sema7A
102 maintained a high level in the subapical region, the protein increasingly accumulated at the
103 base of the hair cell: the Sema7A level at the hair cell base was low at 2 dpf, but increased
104 sharply by 3 dpf and 4 dpf (Fig. 1E; Fig. S1F,G). During this period the hair cells increase in
105 number and mature, whereas the associated sensory axons arborize to contact multiple hair
106 cells and form robust synaptic boutons at their bases (5,23). The progressive enrichment of
107 Sema7A at the hair cell base and sensory-axon interface (Fig. 1F; Movie 1) implicates that
108 Sema7A acts as a potential mediator of contacts between sensory axons and hair cells.

109 **Sema7A patterns sensory axon arborizations**. If Sema7A guides and restricts the sensory
110 arbors around the hair cells clustered in a neuromast, then inactivating Sema7A function should
111 disrupt this process. To test this hypothesis, we obtained a *sema7a* mutant allele
112 (*sema7a*^{sa24691}) with a point mutation that introduces a premature stop codon in the conserved
113 sema domain (Fig. S2A). The homozygous mutant, hereafter designated *sema7a*$^{-/-}$, should
114 lack both the secreted and the membrane-attached forms of Sema7A. The average intensity
115 of Sema7A immunolabeling in hair cells diminished by 61% in *sema7a*$^{-/-}$ larvae (0.34 ± 0.01
116 arbitrary units) in comparison to controls (0.87 ± 0.01 arbitrary units). In a few cases we
117 observed minute accumulations of Sema7A at the subapical region, but little or no protein at
118 the base of the mutant hair cells (Fig. 2A; Fig. S2B).

119 To characterize the impact of the *sema7a*$^{-/-}$ mutation on arbor patterning, we utilized
120 doubly labeled transgenic fish *Tg(myo6b:actb1-EGFP;neurod1:tdTomato)* that marked the hair
121 cells and the sensory axons of the posterior lateral line with distinct fluorophores (25). In control
122 neuromasts, the sensory axons approached, arborized, and consolidated around the bases of
123 clustered hair cells (Fig. 2B). Although the sensory axons approached the hair cells of
124 *sema7a*$^{-/-}$ neuromasts, they displayed aberrant arborization patterns with wayward projections

125 that extended transversely to the organ (Fig. 2C). To quantitatively analyze the arborization
126 morphology, we traced the sensory arbors in three dimensions to generate skeletonized
127 network traces that depict–as pseudocolored trajectories–the increase in arbor length from the
128 point of arborization (Fig. 2D,E).

129 To visualize the hair cell clusters and associated arborization networks from multiple
130 neuromasts, we aligned images of hair cell clusters, registered them at their hair bundles, from
131 neuromasts at 2 dpf, 3 dpf, and 4 dpf. Throughout development, the arborization networks of
132 control neuromasts largely remained within the contours of the hair cell clusters; the few that
133 reached farther nonetheless lingered nearby (Fig. 2F). This result suggests that an attractive
134 cue retained the axons near the sensory organ. In *sema7a*$^{-/-}$ neuromasts, however the neuronal
135 arbors failed to consolidate within the boundaries of hair cell clusters and extended far beyond
136 them (Fig. 2G; Fig. S2C-H; Movie 2).

137 We quantified the distribution of the sensory arbors around the center of the combined
138 hair cell clusters. For both the control and the *sema7a*$^{-/-}$ neuromasts, the arbor densities peaked
139 proximal to the boundaries of the hair cell clusters. Beyond the cluster boundaries, in control
140 neuromasts at 2 dpf, 3 dpf, and 4 dpf the arbor densities fell sharply at respectively 31.7 μm,
141 36.6 μm, and 32.7 μm from the center. In *sema7a*$^{-/-}$ neuromasts of the same ages, the sensory
142 arbors extended respectively 38.5 μm, 51.4 μm, and 56.6 μm from the center (Fig. 2H;
143 Fig. S2I-J; Fig. S5A). Furthermore, we quantified the degree of contact of the sensory arbors
144 to their hair cell clusters in individual neuromasts from both control and *sema7a*$^{-/-}$ mutants. In
145 control neuromasts, the degree of contact was 83 ± 1 % (mean ± SEM) at 2 dpf and 84 ± 1 %
146 at 3 dpf, but significantly increased to 90 ± 1 % at 4 dpf (Fig. 2I; Fig. S5B). This observation
147 indicates that the sensory arbors reinforce their association to the hair cell clusters as
148 neuromasts develop. However, in *sema7a*$^{-/-}$ neuromasts such contact was significantly
149 reduced. Only 69 ± 4 % of sensory arbors at 2 dpf were closely associated with the
150 corresponding hair cell clusters, a value that remained at 67 ± 2 % at both 3 dpf and 4 dpf
151 (Fig. 2I). These findings signify that simultaneous disruption of both signaling modalities of

152 Sema7A fails to restrict sensory arbors within a neuromast and significantly diminishes their
153 contact with hair cells.

154 ***Sema7A^{sec} is a sufficient chemoattractive cue for sensory axon guidance***. Because
155 genetic inactivation of the *sema7a* gene disrupts both signaling modalities of the cognate
156 protein, we could not assess the specific activity of the Sema7A^{sec} diffusive cue in guiding
157 lateral-line sensory axons. To independently verify the potential role of that isoform, we
158 therefore expressed the secreted variant ectopically and investigated the resultant arborization
159 patterns.

160 Analysis of the microcircuit connectivity of the neuromasts has demonstrated bare
161 sensory-axonal terminals in the perisynaptic compartments, where they do not contact the hair
162 cell membrane (8). We speculate that these bare terminals are attracted by a Sema7A^{sec}
163 diffusive cue. To test this hypothesis, we ectopically expressed Sema7A^{sec} protein tagged with
164 the fluorophore mKate2, then analyzed its effect on the morphology of sensory arbors.
165 Fertilized one-cell embryos were injected with the *hsp70:sema7a^{sec}-mKate2* plasmid and
166 raised to 3 dpf. Larvae expressing the transgenesis marker—the lens-specific red fluorescent
167 protein mCherry—were heat-shocked, incubated to allow expression, and subsequently
168 mounted for live imaging. In these larvae, a random mosaic of cells—often embryonic muscle
169 progenitors in the dermomyotome or mature myofibers—expressed the exogenous
170 Sema7A^{sec}-mKate2 protein. We selected only those neuromasts in which an ectopic integration
171 had occurred near the network of sensory arbors (Fig. 3A,B). In all 22 such cases, we observed
172 robust axonal projections from the sensory arbor network toward the ectopically expressing
173 Sema7A^{sec} cells. When the exogenous *sema7a^{sec}* integration occurred in embryonic muscle
174 progenitor cells, which reside in a superficial layer external to the muscle fibers and adjacent
175 to the larval skin (26), the projections were able to form direct contacts with them (Fig. 3C;
176 Movies 3,4). But more often, when mature myofibers expressed the exogenous Sema7A^{sec}
177 deep in the myotome, the axonal projections approached those targets but failed to contact
178 them (Fig. 3D, Movies 5,6). This behavior likely arose because other components in the
179 myotomal niche—including the fibrous epimysium, other myofibers, myoblasts, and immature

180 myotubes whose surroundings are permeable to diverse diffusive cues (27)—physically
181 obstructed direct interaction of the extended neurites with the ectopically expressing myofibers.
182 All 18 of the injected but not heat-shocked control larvae did not express ectopic Sema7A^{sec},
183 and we did not observe aberrant projections from the sensory arbor network (Fig. 3E).

184 To measure the accuracy of the extended axonal projections in finding the ectopic
185 Sema7A^{sec} source, we defined three parameters: (1) the source path, denoted as the linear
186 distance from the point of arborization to the boundary of an ectopically expressing Sema7A^{sec}
187 cell; (2) the projection path, representing the linear distance from the point of arborization to
188 the terminus of the extended projection; and (3) the projection proximity, calculated as the
189 linear distance from the terminus of the extended axonal projection to the nearest boundary of
190 the ectopically expressing Sema7A^{sec} cell (Fig. 3B). We quantified these parameters from 18
191 of the 22 mosaic integration events; in the remainder the extended axonal projections–although
192 following the ectopic source–reentered the posterior lateral line nerve so that identification of
193 the axon terminals was not possible (Fig. S2A-A"; Movie 7). When we plotted the projection
194 path length against the source-path length, we observed a nearly perfect correlation (Fig. 3F).
195 This result signifies that irrespective of the location of the ectopic source–whether proximal or
196 distal to the sensory arbor network–the Sema7A^{sec} cue sufficed to attract axonal terminals from
197 the sensory arbor. Furthermore, the low average projection-proximity length of 3.5 ± 0.7 μm
198 (mean ± SEM) indicated that the extended projection terminals remained either in contact (8 of
199 18) or in the vicinity (10 of 18) of the ectopic Sema7A^{sec} sources (Fig. 3G). These observations
200 together demonstrate that the Sema7A^{sec} diffusive cue is sufficient to provide neural guidance
201 *in vivo*.

202 As the posterior lateral-line ganglion matures, newly formed neurons extend their axonal
203 growth cones along the posterior lateral-line nerve to reach the neuromasts (28). We wondered
204 whether the axonal projections that had yet to be associated with a neuromast could also
205 respond to an ectopic source of Sema7A^{sec}. Indeed, on five occasions in which *sema7a^{sec}*
206 integration had occurred between two neuromasts, we detected neurite extensions from the
207 posterior lateral-line nerve to the ectopic Sema7A^{sec} source (Fig. S3B-B"; Movies 8-10). The

208 responsiveness of the posterior lateral line axons to Sema7A^{sec} might therefore be an intrinsic
209 property of the neurons that does not require the neuromast microenvironment.

210 ***Effect of Sema7a deficiency on synaptic assembly.*** Contact stabilization between an axon
211 and its target cell is essential for synapse formation (29). Neural GPI-anchored proteins can
212 act as regulators of various synaptic-adhesion pathways (30). In the mouse olfactory system,
213 GPI-anchored Sema7A is enriched in olfactory sensory axons and mediates sustained
214 interaction with the dendrites of mitral and tufted cells in the olfactory bulb to establish synapses
215 (15). In the developing mouse brain–particularly in Purkinje cells–GPI-anchored Sema7A
216 instead regulates the elimination of synapses onto climbing fibers (31). The role of anchored
217 Sema7A in regulating synaptic architecture can thus vary according to the cell type and
218 developmental stage. Our demonstration that Sema7A is necessary to consolidate the contact
219 between sensory axons and hair cells during neuromast development suggests a possible role
220 in regulating synaptic structure.

221 Proper synaptogenesis requires the correct spatial organization of the presynaptic and
222 postsynaptic apparatus at the apposition of two cells. At the interface between hair cells and
223 sensory axons, the synaptic network involves two scaffolding proteins in particular: ribeye, a
224 major constituent of the presynaptic ribbons (32), and membrane-associated guanylate kinase
225 (MAGUK), a conserved group of proteins that organize postsynaptic densities (33). Utilizing
226 these scaffolding proteins as markers, we investigated the impact of the *sema7a*$^{-/-}$ mutation on
227 synapse formation. To analyze the distribution of presynaptic densities–immunolabeled with
228 an antibody against the ribeye-associated presynaptic constituent C-terminal binding protein
229 (CTBP) (32)–we counted the number and measured the area of CTBP punctae from multiple
230 neuromasts at several stages of neuromast development (Fig. 4A,B). The CTBP punctae in
231 each hair cell ranged from zero to seven across developmental stages. In the zebrafish's
232 posterior lateral line, the formation of presynaptic ribbons is an intrinsic property of the hair cells
233 that does not require contact with lateral-line sensory axons. However, sustained contact with
234 the sensory axon influences the maintenance and stability of ribbons (34). As neuromasts
235 matured from 2 dpf to 4 dpf, we identified similar distribution patterns with a characteristic

236 increase in the number of CTBP punctae in both control and *sema7a*$^{-/-}$ larvae (Fig. 4C,D). This
237 result implies that the formation of new presynaptic ribbons is not perturbed in the mutants,
238 even though there are on average fewer CTBP punctae (Fig. S4A-C). Measurement of the
239 areas of CTBP punctae also showed similar distributions in both genotypes (Fig. 4E,F) but the
240 average area of presynaptic densities was reduced in the mutants (Fig. S4D-F).

241 Because GPI-anchored Sema7A lacks a cytosolic domain, it is unlikely that Sema7A
242 signaling directly induces formation of presynaptic ribbons. Instead, GPI-anchored Sema7A
243 might induce postsynaptic assembly on the apposed neuronal membrane (15). To characterize
244 the distribution of the postsynaptic aggregates–immunostained with a pan-MAGUK antibody–
245 we performed analyses similar to those above (Fig. 4I,J). At 4 dpf, 68.3 % of the hair cells in
246 the control neuromasts were associated with at least one MAGUK punctum. In the
247 *sema7a*$^{-/-}$ mutant this value fell to 37.5 % (Fig. 4K,L). The average number of MAGUK punctae
248 also declined in the mutants (Fig. S4G-I). As control neuromasts matured from 2 dpf to 4 dpf,
249 the MAGUK punctae showed a shift toward smaller sizes, suggesting that the postsynaptic
250 structure fragmented into smaller entities as observed in other excitatory synapses (35). At
251 4 dpf, 77.5 % of the hair cells in the control neuromasts had postsynaptic densities with areas
252 between 0.10 μm^2 and 0.40 μm^2. In the *sema7a*$^{-/-}$ mutant the corresponding value was only
253 42.5 % (Fig. 4M,N). The average area of MAGUK punctae was also reduced in the mutants
254 compared to the controls (Fig. S4J-L**).** We speculate that the abnormalities in postsynaptic
255 structure arose from reduced contact between the hair cells and the sensory axons in the
256 *sema7a*$^{-/-}$ mutants or from the lack of Sema7A-mediated juxtracrine signaling onto the apposed
257 neurite terminals (15).

258 **Discussion**

259 The specification of neural circuitry requires precise control of the guidance cues that direct
260 and restrict neural arbors at their target fields and facilitate synapse formation. In the lateral-
261 line neuromast of the zebrafish, we have identified Sema7A as an essential cue that regulates
262 the interaction between hair cells and sensory axons. We have discovered dual modes of

263 Sema7A function *in vivo*: the chemoattractive diffusible form is sufficient to guide the sensory
264 arbors toward their target, whereas the membrane-attached form likely participates in the
265 contact-mediated formation and maintenance of synapses. Our results suggest a potential
266 mechanism for hair cell innervation in which a local Sema7A^{sec} diffusive cue consolidates the
267 sensory arbors at the hair cell cluster and the membrane-anchored Sema7A-GPI molecule
268 regulates synapse assembly.

269 Recent studies have begun to dissect the molecular mechanisms of semaphorin
270 signaling in axonal navigation. In explants derived from the murine olfactory bulb, Sema7A
271 interacts directly with integrinβ1 to trigger downstream signaling effectors involving focal
272 adhesion kinase and mitogen-activated protein kinases, which are critical regulators of the
273 cytoskeletal network during axonal pathfinding (4,36). Moreover, the interaction between
274 Sema7A and its receptor plexinC1 activates the rac1-cdc42-PAK pathway, which alters the
275 actin network to promote axonal guidance and synapse formation (15,37). We speculate that
276 lateral-line sensory axons utilize similar mechanisms to sense and respond to Sema7A in the
277 establishment of microcircuits with hair cells.

278 During early development of the posterior lateral line, the growth cones of sensory axons
279 intimately associate with the prosensory primordium that deposits neuromasts along the lateral
280 surface of the larva (38,39). The growth of the sensory fibers with the primordium is regulated
281 by diverse neurotrophic factors expressed in the primordium (40,41). Impairing brain-derived
282 or glial cell line-derived neurotrophic factors and their receptors perturbs directed axonal
283 motility and innervation of hair cells (40,41). Lateral-line hair cells are particularly enriched in
284 brain-derived neurotrophic factor (42) and other chemotropic cues (Fig. S6). Because the
285 sensory axons of *sema7a*$^{-/-}$ mutants reliably branch from the lateral-line nerve to reach hair cell
286 clusters, these chemoattractive factors might compensate in part for the absence of Sema7A
287 function. Although sensory axons are strict selectors of hair cell polarity and form synapses
288 accordingly (5), diverse chemoattractant cues including Sema7A occur uniformly between hair
289 cell polarities (42). It seems likely that unbiased attractive signals bring sensory arbors toward
290 hair cells, after which polarity-specific molecules on hair cell surfaces dictate the final

291 association between axonal terminal and hair cells. Notch-delta signaling and its downstream
292 effectors regulate hair cell polarity and the innervation pattern (6,8,25). It would be interesting
293 to determine whether Notch-mediated polarity signatures on the hair cell's surface can refine
294 the neuromast neural circuitry.

295 **Materials and Methods**

296 **Zebrafish strains and husband**ry. Experiments were performed on 1.5-4 dpf zebrafish larvae
297 in accordance with the standards of Rockefeller University's Institutional Animal Care and Use
298 Committee. Naturally spawned and fertilized eggs were collected, cleaned, staged, and
299 maintained at 28.5 ºC in system-water with 1 µg/mL methylene blue. Wild-type AB and
300 heterozygous mutant *semaphorin7a*^{sa24691} zebrafish were obtained from the Zebrafish
301 International Resource Center. In addition, the following transgenic zebrafish lines were used:
302 *Tg(myo6b:actb1-EGFP)* (43), *Tg(neurod1:tdTomato)* (25), and *TgBAC(neurod1:EGFP)* (44).

303 **Genotyping of mutant fish.** The *semaphorin7a*^{sa24691} allele harbors an A-to-T point mutation
304 in the seventh exon of the *semaphorin7a* gene, which creates a premature stop codon (Fig.
305 S2A). Genomic DNA was isolated from the tail fins of adult *semaphorin7a*^{sa24691} (*sema7a*^{sa91})
306 heterozygous mutant zebrafish. The mutant locus in the genome was PCR amplified using the
307 following primers: sema7a^{sa91}F: 5´-AAAGCTGGAAAGCGAATCAA-3´ and sema7a^{sa91}R:
308 5´-ATATCCAAGGATCCGCCTCT-3´. The 734-base pair amplicons were sequenced, and
309 heterozygous adults were propagated.

310 **Reverse transcription-polymerase chain reactions (RT PCR).** Total RNA was isolated from
311 whole zebrafish larvae by TRIzol extraction followed by DNAse treatment (TURBO DNA-free
312 Ambion). We used thirty 4 dpf zebrafish larvae to isolate total RNA. We generated cDNA
313 libraries using iScript cDNA Synthesis Kit (Bio-Rad). Each transcript was PCR amplified using
314 the following primers: sema7aF: 5´-GGTTTTTCTGAGGCCATTCC-3´, sema7aR1:
315 5´-GGCACTCGTGACAAATGCTA-3´, sema7aR2: 5´-TGTGGAGAAAGTCACAAAGCA-3´
316 (Fig. S1A).

317 **Transient transgenesis with the hsp70l:sema7a^{sec}-mKate2 construct.** The pDNR-LIB
318 plasmid containing the *sema7a^{sec}* coding sequence was purchased from horizon (7140389,
319 Perkin-Elmer). The coding sequence was PCR amplified using the following primers:
320 sema7a^{sec}F:
321 5´-GGGGACAAGTTTGTACAAAAAAGCAGGCTTGATGATTCGACATTATTCT-3´ and
322 sema7a^{sec}R:
323 5´-GGGGACCACTTTGTACAAGAAAGCTGGGTG*CTT*TGTGGAGAAAGTCACAAAGCA-3´.
324 The italicized nucleotides denote the mutated stop codon. The amplicon was then cloned into
325 the pDONR221 vector by BP recombination to generate the middle entry pME-sema7a^{sec}
326 vector. To generate the hsp70:sema7a^{sec}-mKate2 construct, gateway cloning was performed
327 by combining the plasmids p5E-hsp70 (45), pME-sema7a^{sec}, p3E-mKate2-myc no-pA
328 (Addgene, 80812), and pDESTtol2pACrymCherry (Addgene, 64023) with LR Clonase II Plus
329 (Invitrogen). Verified constructs (25 ng/µl plasmid DNA) were injected with Tol2 Transposase
330 mRNA (approximately 25 ng/µl) into one-cell embryos. The transiently transgenic larvae—
331 identified by the expression of red fluorescent protein (mCherry) in their lenses—were raised
332 till 3 dpf, heat-shocked in a water bath at 37 ºC for 1 hr, incubated at 28 ºC for 1 hr to allow
333 expression, and subsequently mounted for live imaging.

334 **Microscopy and volumetric rendering of living neuronal arbors and cells.** Living larvae
335 were dechorionated, anaesthetized in 600 µM 3-aminobenzoic acid ethyl ester
336 methanesulfonate in system-water with 1 µg/mL methylene blue, and mounted in 1 % low-
337 melting-point agarose on a glass-bottom MetTek dish at specific stages. The larvae were
338 maintained at 28 °C during imaging in a temperature-controlled stage top chamber (OKO Lab
339 UNO-T). Images at successive focal depths were captured at 200 nm intervals and
340 deconvolved with Microvolution software in ImageJ (NIH). The three-dimensional datasets
341 were processed and volume-rendered with the surface evolver and filament-tracer tools in
342 Imaris (Bitplane, Belfast, UK). The Imaris workstation was provided by the Rockefeller
343 University Bio-imaging Resource Center.

344 **Immunofluorescence microscopy.** For the immunofluorescence labeling of wholemounted
345 wild-type control and *sema7a*$^{-/-}$ larvae, 1.5-4 dpf larvae were fixed overnight at 4 °C in 4 %
346 formaldehyde in phosphate-buffered saline solution (PBS) with 1 % Tween-20 (1 % PBST).
347 Larvae were washed four times with 1 % PBST for 15 min each, then placed for 2 hr in blocking
348 solution containing PBS, 2 % normal donkey serum (NDS), 0.5 % Tween-20, and 1 % BSA.
349 Primary antibodies were diluted in fresh blocking solution and incubated with the specimens
350 overnight at 4 °C. The primary antibodies were goat anti-Sema7A (1:200; AF1835, R&D
351 Systems) (14), rabbit anti-myosin VI (1:200; Proteus 25-6791), murine anti-GM130 (1:200;
352 610822, BD Transduction Laboratories), murine anti-CTBP (1:200; B-3, SC-55502, Santa Cruz
353 Biotech), and rabbit anti-mCherry (1:200; GTX128508, GeneTex). Larvae were washed four
354 times with 0.1% PBST for 15 min each. Alexa Fluor-conjugated secondary antibodies
355 (Invitrogen, Molecular Probes) applied overnight at 1:200 dilutions in 0.2 % PBST included anti-
356 rabbit (488 nm), anti-goat (555 nm), and anti-mouse (647 nm). Larvae were then washed four
357 times in 0.2 % PBST for 15 min each and stored at 4 °C in VectaShield (Vector Laboratories).
358 For the immunofluorescence labeling of postsynaptic density in wholemounted wild-type
359 control and *sema7a*$^{-/-}$ larvae, 2-4 dpf larvae were fixed with 4 % formaldehyde in PBS for
360 4.5-6 hr at 4 °C. Larvae were washed five times with 0.01 % PBST for 5 min each and then
361 rinsed in distilled water for 5 min. The larvae were permeabilized with ice-cold acetone at -20 °C
362 for 5 min. They were rinsed in distilled water for 5 min, washed five times with 0.01 % PBST
363 for 5 min each, and blocked overnight with PBS buffer containing 2 % goat serum and 1 %
364 BSA. Murine anti-pan-MAGUK antibody (1:500; IgG1 NeuroMab, K28.86, 75-029) was diluted
365 in PBS containing 1 % BSA, added to the larvae, and incubated for 3 hr at room temperature.
366 Larvae were washed five times for 5 min each with 0.01 % PBST. Alexa Fluor 555-conjugated
367 anti-mouse secondary antibody (1:1000) diluted in PBS containing 1 % BSA was added to the
368 larvae and incubated for 2 hr at room temperature. Larvae were washed five times with 0.01 %
369 PBST for 5 min each, rinsed in distilled water for 5 min, and stored at 4 °C in VectaShield
370 (Vector Laboratories).

371 Posterior segments of fixed larvae were mounted on a glass slide and imaged with a
372 microlens-based, super-resolution confocal microscope (VT-iSIM, VisiTech international)
373 under 60X and 100X, silicone-oil objective lenses of numerical apertures 1.30 and 1.35,
374 respectively. Images at successive focal depths were captured at 200 nm intervals and
375 deconvolved with the Microvolution software in ImageJ.

376 **Measurement of Sema7A intensity.** The average Sema7A fluorescence intensities of the hair
377 cells from 1.5 dpf, 2 dpf, 3 dpf, and 4 dpf neuromasts were measured by determining the mean
378 gray level within each hair cell labeled by actin-GFP expression. The intensity distribution of
379 Sema7A protein along the apicobasal axis of the hair cell was measured using the line profile
380 tool in ImageJ (Fig. S1F). Because hair cell lengths differed among samples, lines were drawn
381 with 2 µm widths and varying lengths of 6-8 µm. For each hair cell, apicobasal length was
382 scaled from 0 to 100 arbitrary units and the intensity values from 0 to 1 arbitrary units.

383 **Generation of skeletonized networks.** The labeled sensory axons were traced in three
384 dimensions with ImageJ's semi-automated framework, SNT (46). Each trace depicts the
385 skeletonized form of the posterior lateral-line nerve, the posterior lateral-line branch, and the
386 point of arborization from which the sensory arbors radiate to contact the hair cells (Fig. 2D,E).
387 The three-dimensional pixels or voxels obtained from the skeletonized sensory arbor traces
388 were processed using custom code written in Python for visual representation and quantitative
389 analysis.

390 **Generation of combined hair cell clusters and the corresponding combined skeletonized**
391 **networks.** The hair cell clusters of neuromasts from each developmental stage were aligned
392 by the centers of their apices, which were identified by the hair bundles, and overlayed to
393 generate combined hair cell clusters using custom Python code. The associated skeletonized
394 sensory-arbor traces at each developmental stage were aligned similarly using custom Python
395 code. The details of the procedures are available upon request and the corresponding code is
396 available on GitHub.

397 **Quantification of sensory arbor distributions around hair cell clusters.** The region from
398 the center of the combined hair cell cluster to 60 µm in the post-cluster region was divided into
399 3600 concentric sections of equal area (Fig. S5A). Each section, as depicted with a distinct
400 color shade, had an area of π μm^2. Sensory arbor density was defined as Log_{10}[(Area occupied
401 by the arbors in each section)/ (Area of each section)]. The arbor density was then plotted as
402 a histogram against distance from the center of the combined hair cell cluster. Each bin of the
403 histogram represents an area of π μm^2. The histograms were finally represented as density
404 trace graphs with Kernel Density Estimation (KDE) in Python.

405 **Quantification of contact between sensory arbors and hair cell clusters.** For each hair cell
406 cluster, the voxels of the sensory arbor traces that were inside or within 0.5 μm—the average
407 neurite radius—of the cluster boundary were denoted as arbors in contact with their
408 corresponding hair cell cluster (Fig. S5B). The percentage of arbors in contact with each hair
409 cell cluster was defined as: (Number of voxels that remained inside the cluster boundary/Total
410 number of voxels in the arbor)X100. The data were analyzed through an automated pipeline
411 with custom code.

412 **Quantification of aberrant sensory arborization in ectopic Sema7A^{sec} expression.** The
413 sensory arbor networks were traced in three dimensions with SNT. The surface of each of the
414 ectopically expressing Sema7A^{sec}-mKate2 cells was represented by a single point that was
415 closest to the terminal point of the guided neurite. Distances between two points were
416 calculated using standard mathematical operations.

417 **Statistical analysis.** Data visualization and statistical analysis were conducted with GraphPad
418 Prism (Version 9). The Mann-Whitney test was used for hypothesis testing, and the statistical
419 details are given in the respective figure legends.

420 **Data and code availability.** Owing to size restrictions, the experimental image data have not
421 been uploaded to a repository but are available from the corresponding author on request. The

code generated during this study is available on GitHub (https://github.com/agnikdasgupta/Sema7A_regulates_neural_circuitry).

Acknowledgments. The authors thank Adrian Jacobo, Caleb Reagor, and Nicolas Velez for valuable discussions and data processing. Samantha Campbell and Anna Kaczynska provided expert fish husbandry. Katie Kindt kindly provided various strains of zebrafish. Image processing benefitted from facilities at the Bio-Imaging Resource Center. A.D. was supported by a Kavli Neural Systems Institute Postdoctoral Fellowship from Rockefeller University. S.P.P. and L.M.S. were supported by Howard Hughes Medical Institute, of which A.J.H. is an Investigator.

Author Contributions

A.D. initiated the project, conducted experiments, and quantified results. S.P.P. developed the Python codes for image analysis and quantified results. L.M.S. conducted preliminary experiments. A.D. wrote the paper with contributions from A.J.H.

Declaration of Interests

The authors declare no competing interests.

438 **Figure Legends**

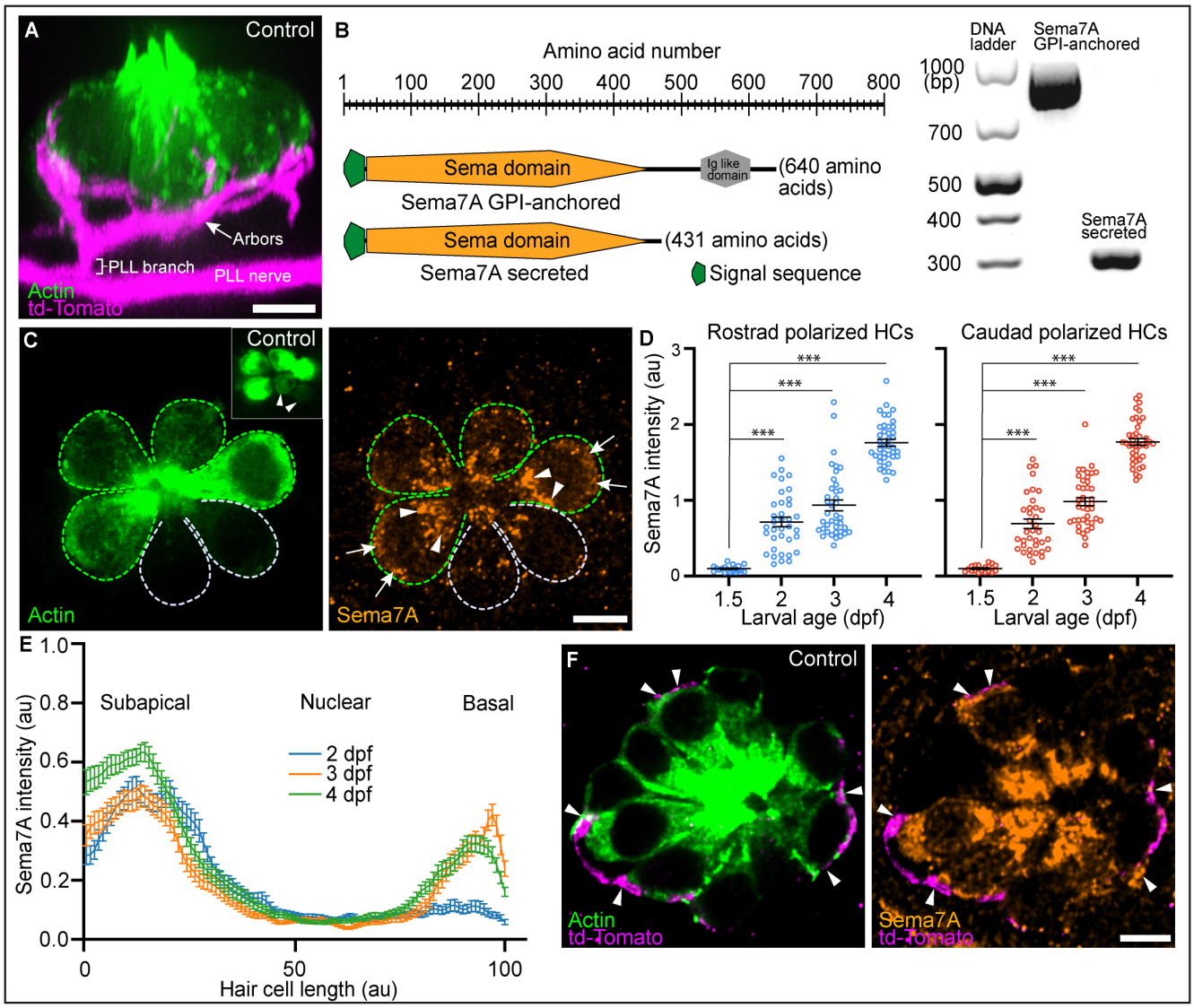

439
440

441 **Figure 1. Expression of Semaphorin7A in the zebrafish's lateral line.** (A) A volumetric
442 rendering of a PLL neuromast depicts the sensory axons (magenta) that branch from the lateral
443 line nerve to arborize around the basolateral surface of the hair cell cluster (green). Additional
444 cell types in the neuromast are not labeled. Larval age, 3 dpf. (B) A schematic drawing of the
445 two variants of the Sema7A protein molecule depicts the full-length GPI-anchored form and the
446 smaller, potentially secreted form. Both the molecules include a signal sequence (green) and
447 a conserved sema domain (orange). Gel-based RT-PCR analysis indicates the presence of

448 both the variants in developing larva. (C) A surface micrograph of a neuromast at 3 dpf depicts
449 two pairs of mature hair cells (green dashed lines) and a pair of immature hair cells (grey
450 dashed lines). Inset: among the three pairs of hair cell apices, the immature pair is indicated
451 by arrowheads. Immunolabeling reveals that the Sema7A protein (orange) occurs consistently
452 at the subapical region (arrowheads) and at the basolateral surface (arrows) of a hair cell. In
453 this and in each of the subsequent neuromast images, anterior is to the left and ventral to the
454 top. (D) A plot quantifies developmental changes in the average Sema7A intensity in both
455 rostrally and caudally polarized hair cells of neuromasts from 1.5 dpf to 4 dpf. The data stem
456 from 18, 36, 39, and 40 hair cells in neuromasts of respectively 1.5 dpf, 2 dpf, 3 dpf, and 4 dpf
457 larvae. (E) A plot quantifies the distribution of average Sema7A intensity along the hair cell's
458 apicobasal axis. The results stem from 52, 57, and 54 hair cells of neuromasts from 2 dpf,
459 3 dpf, and 4 dpf larvae. (F) An immunofluorescence image at the nuclear level of a 4 dpf
460 neuromast shows the contact of the sensory arbors (magenta) with the basolateral surface of
461 the hair cells (green). Immunolabeling for Sema7A (orange) reveals enrichment of the protein
462 at the hair cell bases and sensory-axon interfaces (arrowheads). HC, hair cell; Scale bars,
463 5 μm; au, arbitrary unit; means ± SEMs; *** implies $p < 0.001$.
464

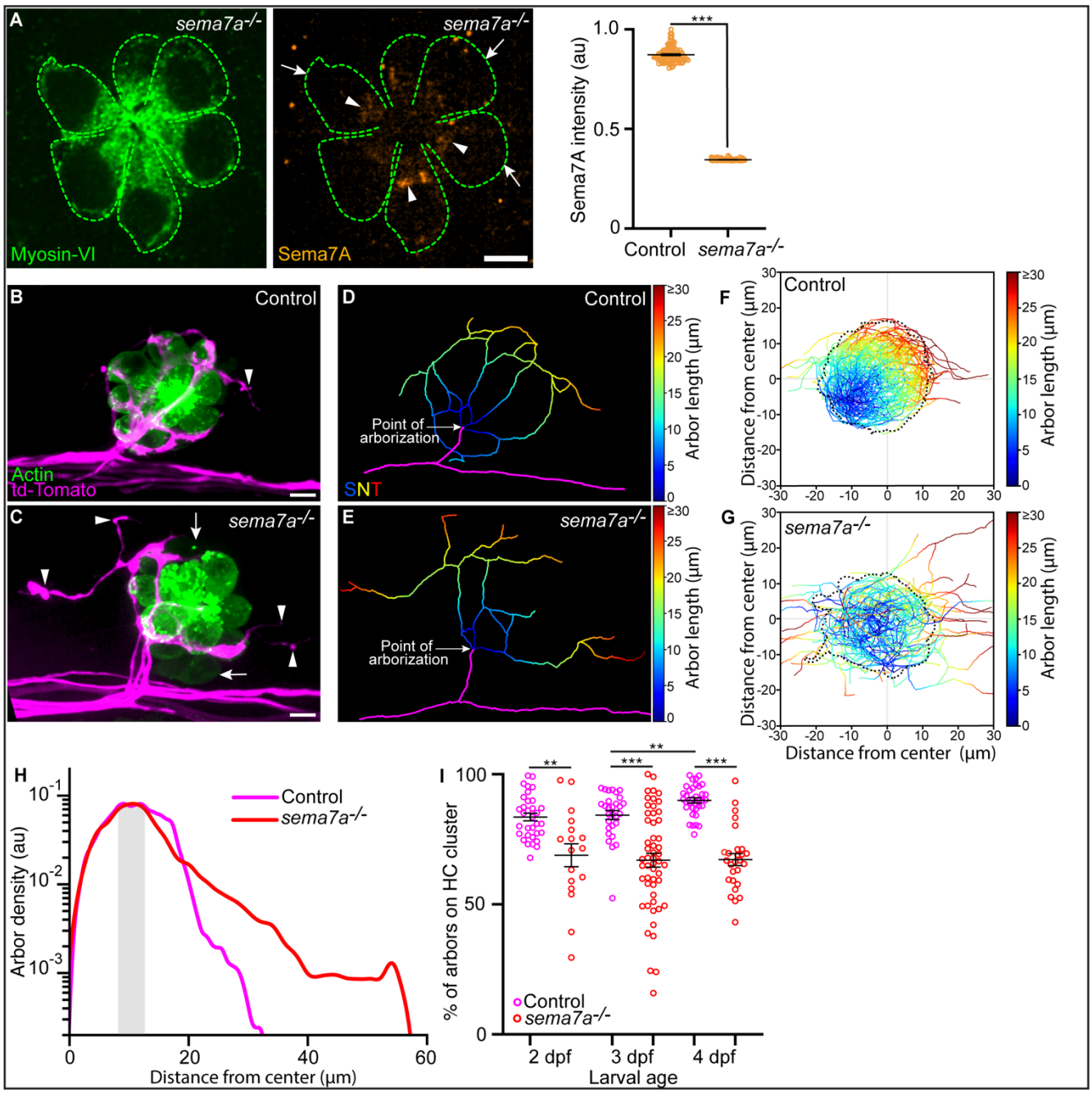

465 **Figure 2. *sema7a*$^{-/-}$ mutants display aberrant sensory axon arborizations.** (A) In a
466 micrograph of a 3 dpf *sema7a*$^{-/-}$ neuromast, Myosin VI (green) marks the hair cells (green
467 dashed lines) in which the level of Sema7A (orange) is highly reduced, with sporadic
468 localization in the subapical region (arrowheads) and none in the basolateral (arrow) region. A
469 plot of normalized Sema7A intensity from 99 control and 100 *sema7a*$^{-/-}$ hair cells quantitates

470 the effect. (B,C) Surface views of a control and a *sema7a*$^{-/-}$ neuromast at 4 dpf depict the
471 interaction of the sensory arbors (magenta) with hair cell clusters (green). In the control, the
472 arbors intimately contact the hair cells, with a few exceptions (arrowhead). In the *sema7a*$^{-/-}$
473 mutant, the arbors direct many aberrant projections (arrowheads) away from the hair cell
474 cluster. The two immature hair cell pairs in the *sema7a*$^{-/-}$ neuromast are indicated by arrows.
475 (D,E) Skeletonized networks portray the three-dimensional topology of the sensory arbors from
476 the control and the *sema7a*$^{-/-}$ neuromasts depicted in panels B and C. The pseudocolored
477 trajectories depict the increase in arbor contour length from each point of arborization, defined
478 as the point at which the lateral line branch (magenta) contacts hair cell cluster.
479 (F,G) Micrographs depict the skeletonized networks of the combined 4 dpf hair cell clusters,
480 whose centers are located at (0,0). The X- and Y-coordinates represent the anteroposterior
481 (AP) and the dorsoventral (DV) axes of the larva, respectively. Positive values of the X- and
482 Y-coordinates represent the posterior and ventral directions, respectively. Combined
483 skeletonized network traces from 27 control and 27 *sema7a*$^{-/-}$ mutant neuromasts are
484 represented. H) The plot denotes the densities of the sensory arbors around the center of the
485 combined hair cell clusters for 35 control (magenta) and 27 *sema7a*$^{-/-}$ (red) neuromasts at 4 dpf.
486 The shaded area marks the region proximal to the boundary of the combined hair cell cluster.
487 (I) The plot quantifies the degree of contact of the sensory arbors to their hair cell clusters in
488 individual neuromasts from both control (magenta) and *sema7a*$^{-/-}$ mutants (red), each point
489 represents a single neuromast. Thirty-three, 29, and 35 neuromasts were analyzed from 2 dpf,
490 3 dpf, and 4 dpf control larvae, respectively. Seventeen, 53, and 27 neuromasts were analyzed
491 from 2 dpf, 3 dpf, and 4 dpf *sema7a*$^{-/-}$ mutant larvae, respectively. HC, hair cell; Scale bars,
492 5 μm; au, arbitrary unit; means ± SEMs; *** implies $p < 0.001$; ** signifies $p < 0.01$.
493

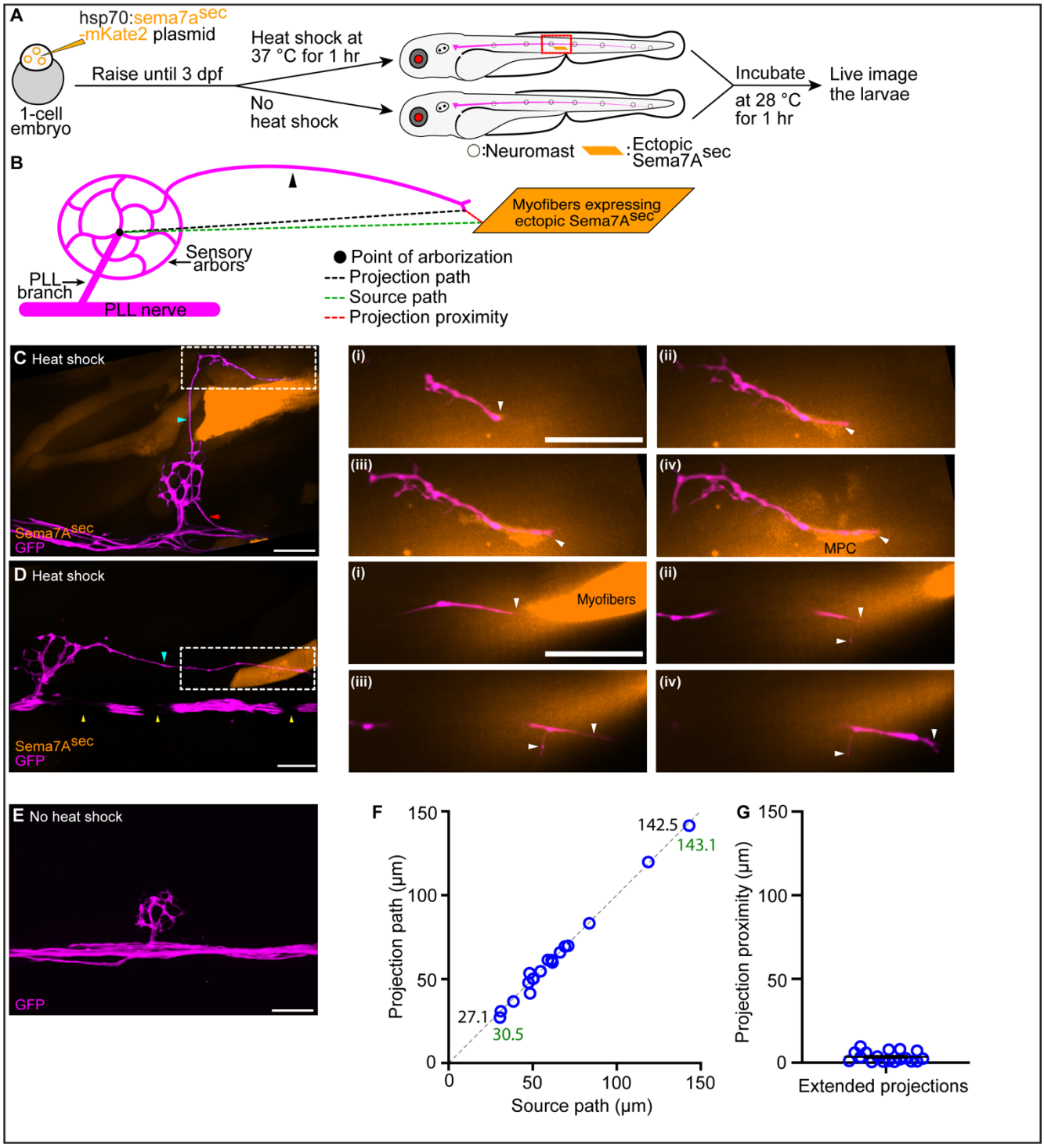

494 **Figure 3. Ectopic Sema7A^sec diffusive cue provides neural guidance *in vivo*.** (A) A
495 diagrammatic overview depicts the generation of a transgenic animal that expresses the
496 Sema7A^sec protein ectopically under the control of a thermally inducible promoter. Larvae with

497 ectopic myotomal-integration near the network of sensory arbors (red line) were imaged to
498 analyze arbor morphology. (B) A schematic drawing of a sensory arbor from a heat-shocked
499 larva depicts an extended axonal projection (arrowhead) that reaches toward the myofibers
500 expressing the ectopic Sema7A^{sec} protein. Parameters that quantitate the accuracy of the
501 extended axonal projections toward the ectopic Sema7A^{sec} sources are denoted. (C) In a
502 micrograph of an ectopically expressing Sema7A^{sec} (orange) larva, the sensory arbor
503 (magenta) extends two aberrant axonal projections. One elongates (cyan arrowhead) along
504 the somite boundary to reach and contact an ectopically integrated muscle progenitor cell
505 (white dashed line) and the other (red arrowhead) reenters the posterior lateral line nerve while
506 following a second ectopic source. The through-focus scan (i–iv) from the epidermis to the
507 dermomyotome reveals the intimate contact between the aberrant sensory arbor (arrowheads)
508 and the muscle progenitor cell. MPC, muscle progenitor cell. (D) In a micrograph of an
509 ectopically expressing Sema7A^{sec} (orange) larva, the sensory arbor (magenta) extends a single
510 aberrant axonal process (cyan arrowhead) to reach ectopically integrated myofibers (white
511 dashed line). The through-focus scan (i–iv) from the epidermis to the deep myotome reveals
512 the proximal association of the aberrant sensory arbor (arrowheads) to the myofibers.
513 Melanocytes (yellow arrowhead) along the horizontal myoseptum intermittently block the
514 visibility of the lateral line nerve. (E) An injected, but not heat-shocked, control larva does not
515 express ectopic Sema7A^{sec} and does not show aberrant projection from the sensory arbor.
516 (F) A plot demonstrates the accuracy of 18 extended axonal arbors in finding ectopic
517 Sema7A^{sec} sources. Each circle represents a single ectopic integration event. The two pairs of
518 numbers represent the minimal and maximal lengths of the projection path (black) and its
519 corresponding source path (green). (G) A plot quantitates the distribution of projection-
520 proximity length from 18 ectopic integration events. Scale bars, 20 μm; means ± SEMs.
521

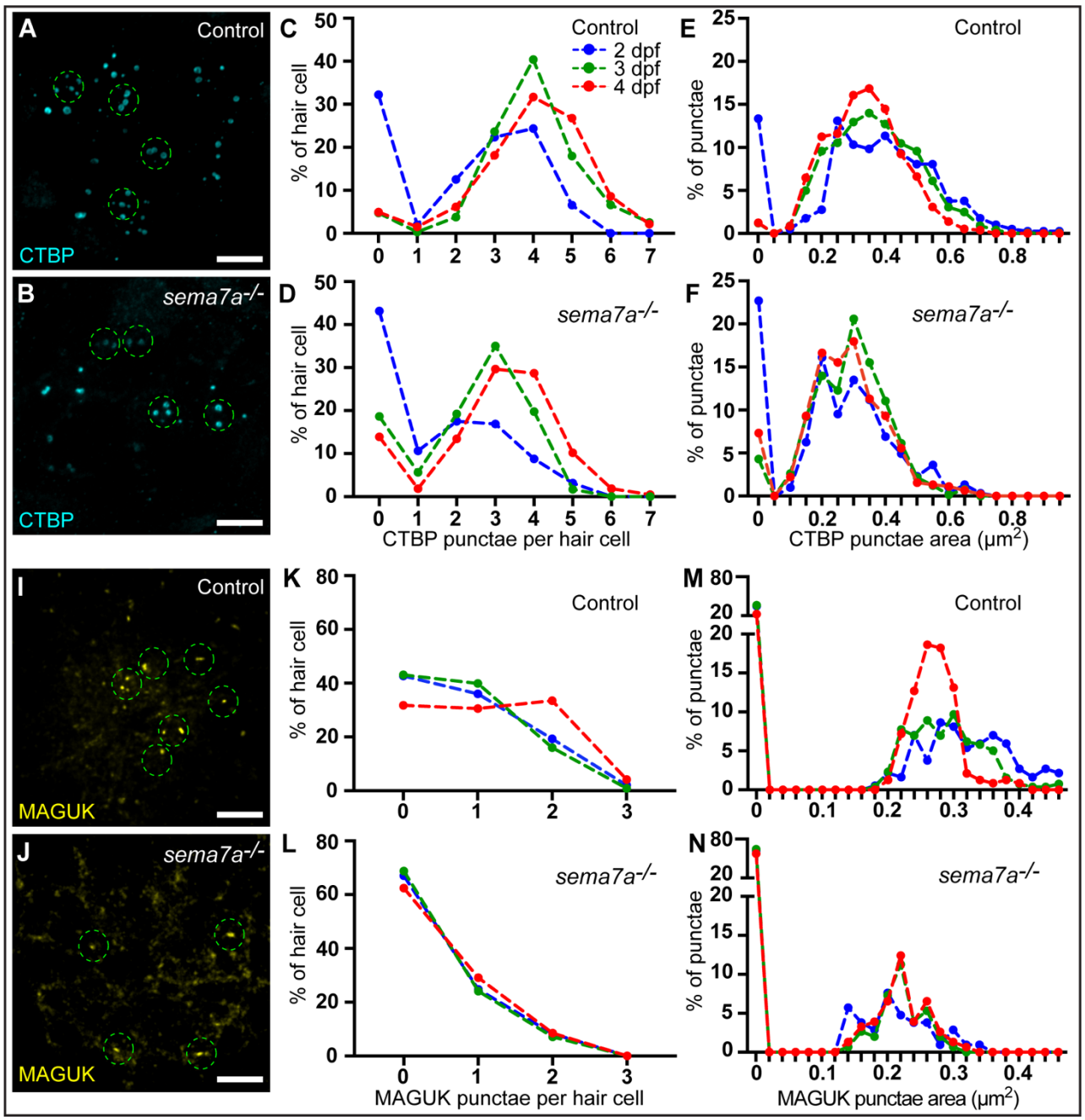

522 **Figure 4. Sema7a deficiency impairs synaptic assembly.** (A,B) Maximal-intensity
523 projections of micrographs from a control and a *sema7a*$^{-/-}$ neuromast depict the presynaptic
524 aggregates marked by CTBP (cyan). The approximate hair cell basal region is outlined by
525 dashed green circles. (C-F) Plots quantitate the numbers of presynaptic aggregates (C,D) and
526 their areas (E,F), in each hair cell across developmental stages. One hundred and fifty-two,

527 317, and 325 hair cells were analyzed from 2 dpf, 3 dpf, and 4 dpf control larvae, respectively.
528 One hundred and sixty, 216, and 177 hair cells were analyzed from 2 dpf, 3 dpf, and 4 dpf
529 *sema7a*$^{-/-}$ mutant larvae, respectively. (I,J) Maximal-intensity projections from micrographs of
530 a control and a *sema7a*$^{-/-}$ neuromast depict the postsynaptic aggregates marked by MAGUK
531 (yellow). The approximate hair cell basal region is outlined by dashed green circles. (K,N) Plots
532 quantitate the numbers of postsynaptic aggregate (K,L) and their areas (M,N), in each hair cell
533 across developmental stages. One hundred and fifty, 218, and 167 hair cells were analyzed
534 from 2 dpf, 3 dpf, and 4 dpf control larvae, respectively. Ninety-seven, 141, and 141 hair cells
535 were analyzed from 2 dpf, 3 dpf, and 4 dpf *sema7a*$^{-/-}$ mutant larvae, respectively. Scale bars,
536 5 μm.
537

538 **Supplementary Figure Legends**

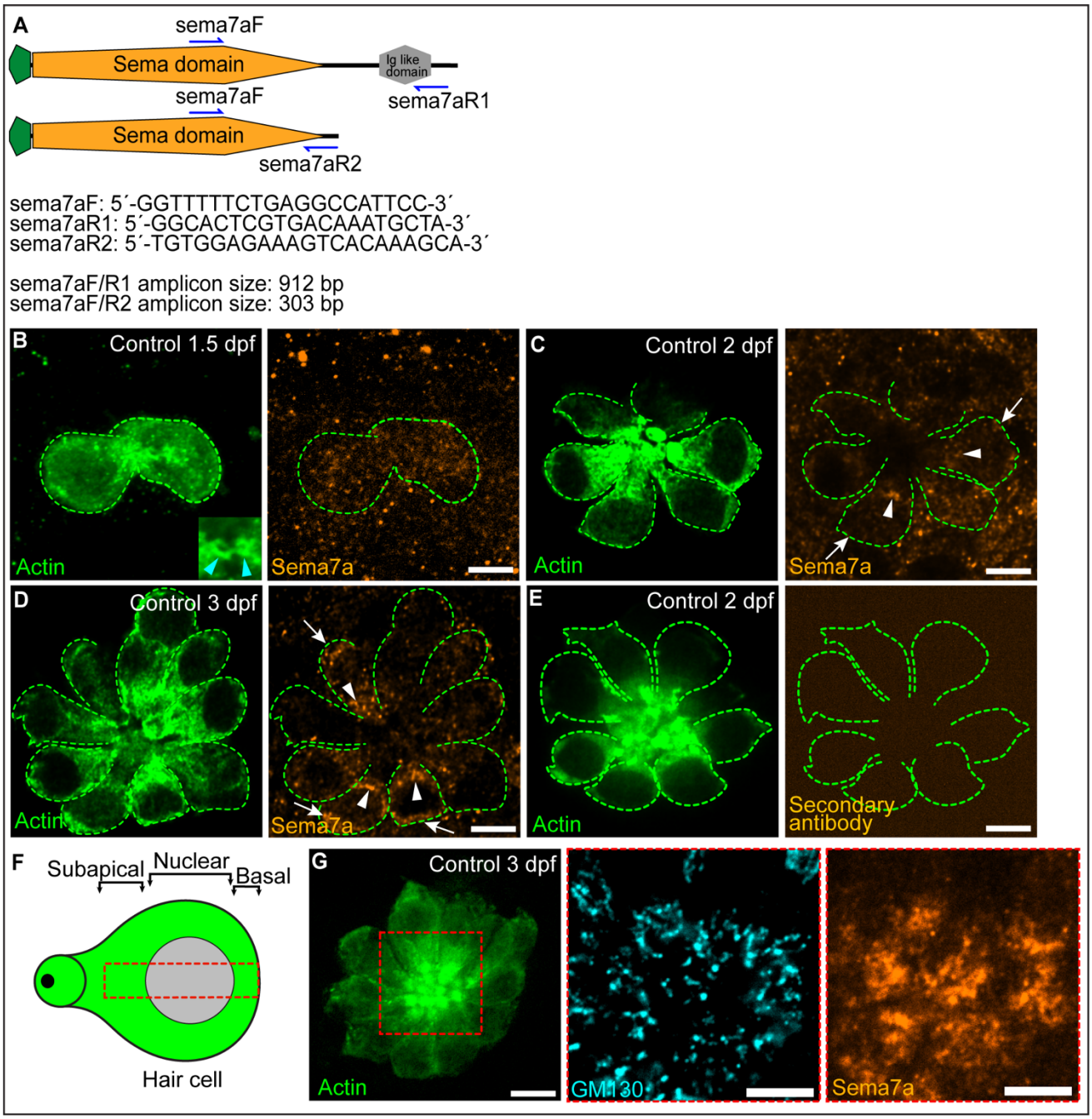

539 **Supplementary Figure 1. Expression of Semaphorin7A in the lateral line neuromast.**
540 (A) Distinct sets of primers (arrows) identify the two variants of the Sema7A protein molecule.
541 (B-D) Surface micrographs show hair cells marked with actin-GFP (green dashed lines) and
542 the localization of Sema7A protein (orange) in the subapical (arrowheads) and basal regions

543 (arrows) of the corresponding hair cells from neuromasts of developing control larvae. The
544 inset in panel B depicts the apices of the immature hair cell pair. (E) Immunolabeling with only
545 the secondary antibody fails to detect any Sema7A signal. (F) A schematic diagram of a single
546 hair cell depicts the three distinct regions along the apicobasal axis of the cell. Sema7A
547 intensity was measured along this apicobasal axis (red dashed line). (G). A surface micrograph
548 depicts hair cells (green, left) whose subapical region (red dashed line) harbors the Golgi
549 network (cyan, middle) where the Sema7A protein is enriched (orange, right). Scale bars, 5 μm.

550

551 **Supplementary Movie 1. Sema7A is enriched at the hair cell base and sensory-axon**
552 **interface**. A through-focus scan of a 4 dpf control neuromast depicts the hair cells (green) that
553 are innervated by the sensory axons (magenta) at their basolateral surfaces where the Sema7A
554 protein (orange) is highly enriched. Scale bar, 5 μm.
555

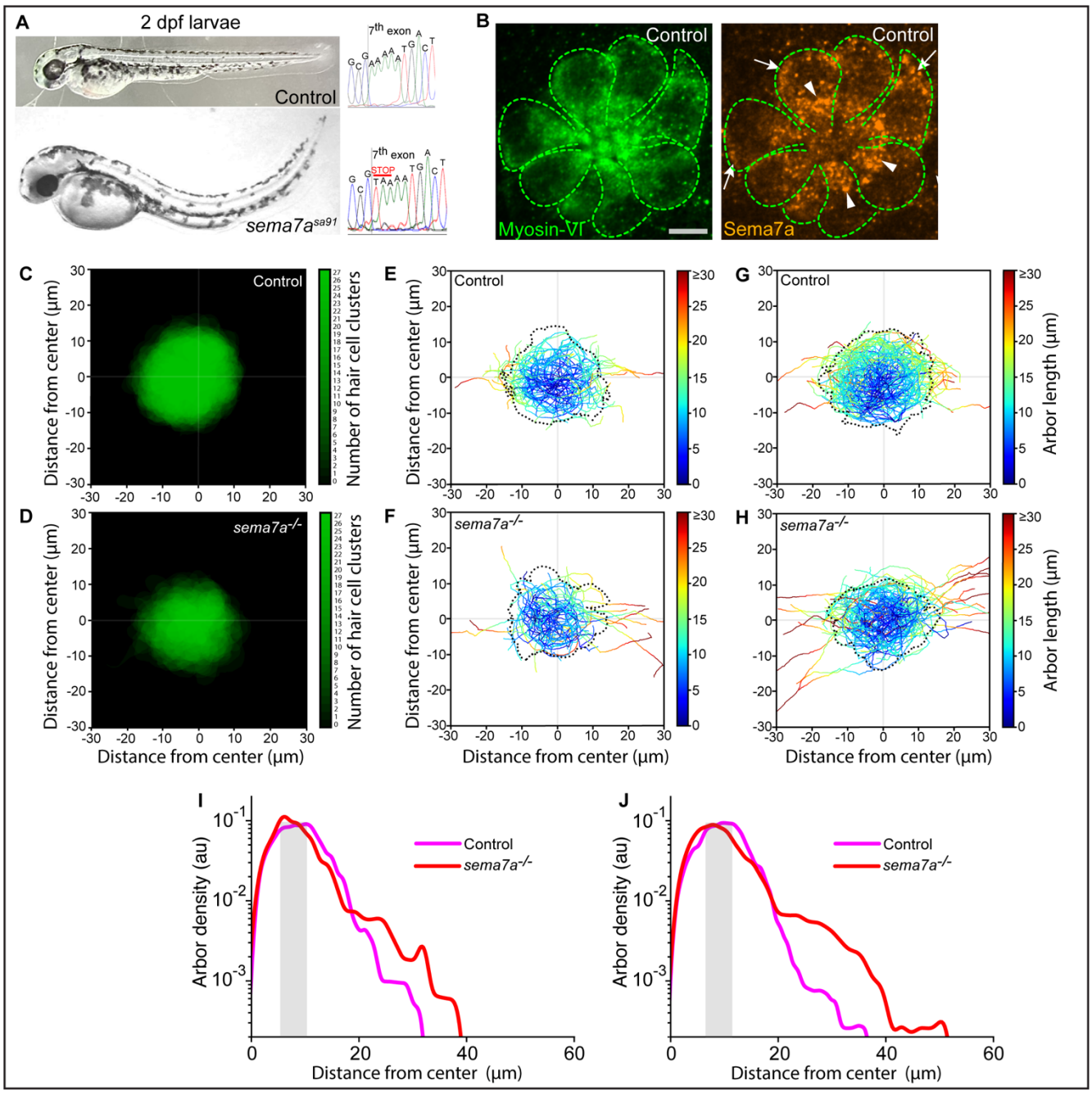

556

557 **Supplementary Figure 2. *sema7a*$^{-/-}$ mutants exhibit aberrant sensory-axon arborization**
558 **throughout development.** (A) Micrographs depict the overall morphologies and *sema7a*
559 genomic profiles of 2 dpf control (top) and *sema7a*$^{-/-}$ larvae (bottom). (B) In a surface
560 micrograph of a 3 dpf control neuromast, myosin VI (green) marks hair cells (green dashed
561 lines). Sema7A (orange) protein is highly enriched in the subapical region (arrowheads) and
562 basolateral (arrow) region of the hair cells. (C,D) Micrographs depict combined 4 dpf hair cell
563 clusters, each of whose centers arise located at (0,0). The X- and Y-coordinates represent the
564 anteroposterior (AP) and dorsoventral (DV) axes of the larva, respectively. Positive values of

565 the X- and Y-coordinates represent posterior and ventral directions, respectively. Combined
566 hair cell clusters from 27 control and 27 *sema7a*$^{-/-}$ mutant neuromasts are represented.
567 (E,F) Micrographs depict the skeletonized networks of the combined 2 dpf hair cell clusters
568 from 17 control and 17 *sema7a*$^{-/-}$ mutant neuromasts. (G,H) Micrographs depict the
569 skeletonized networks of the combined 3 dpf hair cell clusters from 29 control and 29
570 *sema7a*$^{-/-}$ mutant neuromasts. (I) A plot quantitates the densities of the sensory arbors around
571 the center of the combined hair cell clusters for 33 control (magenta) and 17 *sema7a*$^{-/-}$ (red)
572 neuromasts at 2 dpf. The shaded area marks the region proximal to the boundary of the
573 combined hair cell cluster. (J) A plot quantitates the densities of the sensory arbors around the
574 center of the combined hair cell clusters for 29 control (magenta) and 53 *sema7a*$^{-/-}$ (red)
575 neuromasts at 3 dpf. The shaded area marks the region proximal to the boundary of the
576 combined hair cell cluster. Scale bar, 5 μm; au, arbitrary units.

577

578 **Supplementary Movie 2. Three-dimensional arborization patterns in control and**
579 ***sema7a*$^{-/-}$ neuromasts.** Lateral views depict **t**hree-dimensionally rendered combined
580 skeletonized network traces from 27 control and 27 *sema7a*$^{-/-}$ mutant neuromasts.
581

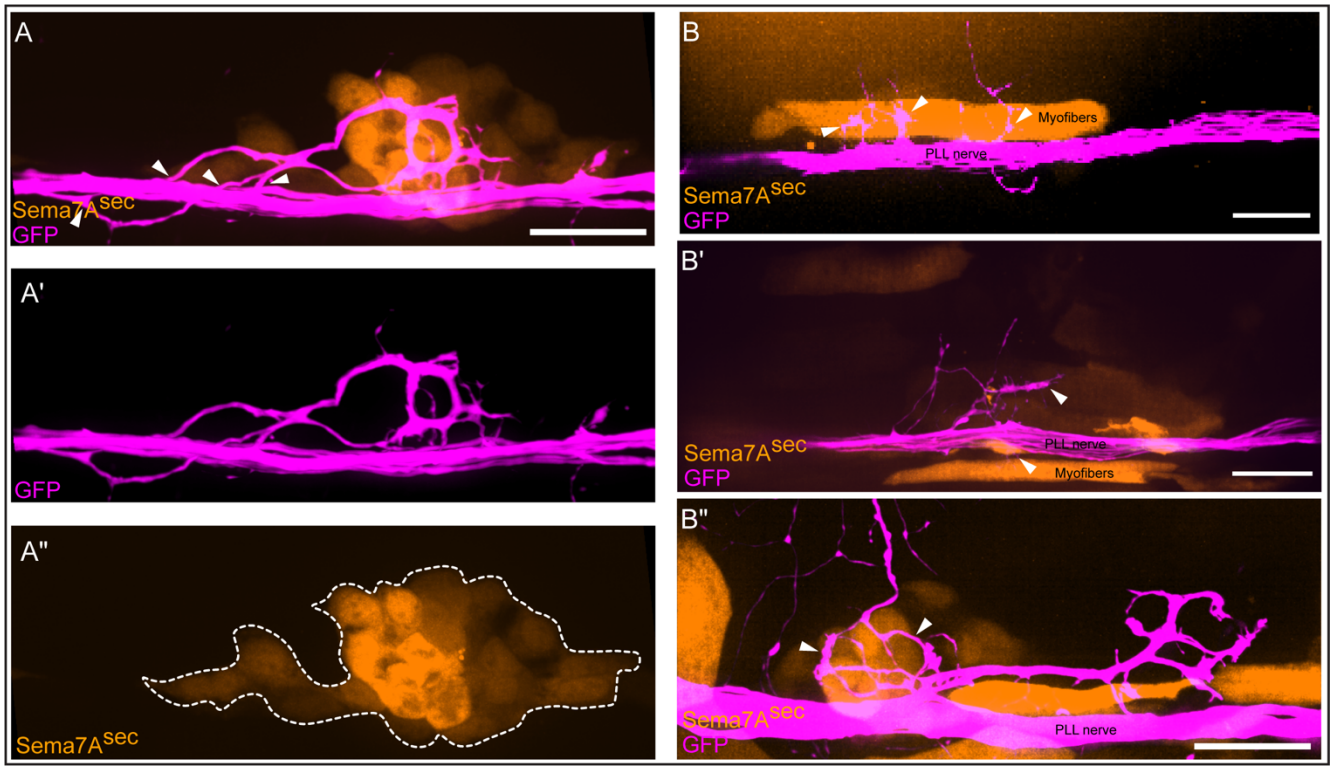

582

583 **Supplementary Figure 3. Ectopic Sema7A^{sec} diffusive cues induce aberrant neural**
584 **arborizations.** (A-A") In a micrograph of an ectopically expressing Sema7A^{sec} (orange) larva,
585 the sensory arbors (magenta) extend multiple aberrant axonal projections (arrowheads) that
586 reenter the lateral line nerve while following an ectopic Sema7A source. Maximal-intensity
587 projections of the sensory arbors and the ectopically expressing Sema7A cells (white dashed
588 line) are shown in A' and A", respectively. (B-B") Micrographs depict three individual incidents
589 of ectopic *sema7a^{sec}* (orange) integrations that occurred distant from neuromasts. In each
590 case, a set of myofibers expresses the ectopic Sema7A^{sec} protein that induces neurite
591 extensions (arrowheads) from the lateral line nerve (magenta) toward itself. Scale bars, 20 μm.
592

593 **Supplementary Movie 3. Sensory axonal projections contact an embryonic muscle**
594 **progenitor cell expressing Sema7A^{sec}.** A through-focus scan of a 3 dpf larva depicts a
595 muscle progenitor cell in the dermomyotome that expresses the ectopic Sema7A^{sec} (orange)
596 and the sensory axonal projection (magenta) that makes intimate contact with it.

597

598 **Supplementary Movie 4. Volumetric surface reconstruction of a sensory arbor and an**
599 **embryonic muscle progenitor expressing Sema7A^{sec}.** Reconstruction of the muscle
600 progenitor cell (orange) at 3 dpf reveals its intimate association with an attracted sensory arbor
601 (magenta).

602

603 **Supplementary Movie 5. Sensory axonal projections remain in proximity to myofibers**
604 **expressing Sema7A^{sec}.** A through-focus scan of a 3 dpf larva depicts mature myofibers
605 expressing exogenous Sema7A^{sec} deep in the myotome (orange) and the sensory axonal
606 projection (magenta) that remains nearby.

607

608 **Supplementary Movie 6. Volumetric surface reconstruction of a sensory arbor and the**
609 **mature myofibers expressing Sema7A^{sec}.** Reconstruction of mature myofibers expressing
610 ectopic Sema7A^{sec} (orange) at 3 dpf shows their close association with the attracted sensory
611 arbors (magenta).

612

613 **Supplementary Movie 7. Aberrant axonal projections reenter the lateral line nerve while**
614 **following an ectopic Sema7A^{sec} source.** A through-focus scan of a 3 dpf larva depicts cells
615 expressing exogenous Sema7A^{sec} (orange) that guides the aberrant sensory axonal projection
616 (magenta) back into the lateral line nerve. Scale bar, 20 μm.

617

618 **Supplementary Movie 8, 9, and 10. Ectopic Sema7A^{sec} expression induces aberrant**
619 **neurite projections from the lateral line nerve.** Through-focus scans of 3 dpf larvae depict
620 three individual incidents of ectopic *sema7a^{sec}* (orange) integrations that occurred distant from
621 the neuromasts. In each case, myofibers express ectopic Sema7A^{sec} protein that attracts
622 neurite extensions (arrowheads) from the lateral line nerve (magenta). Scale bars, 20 μm.
623

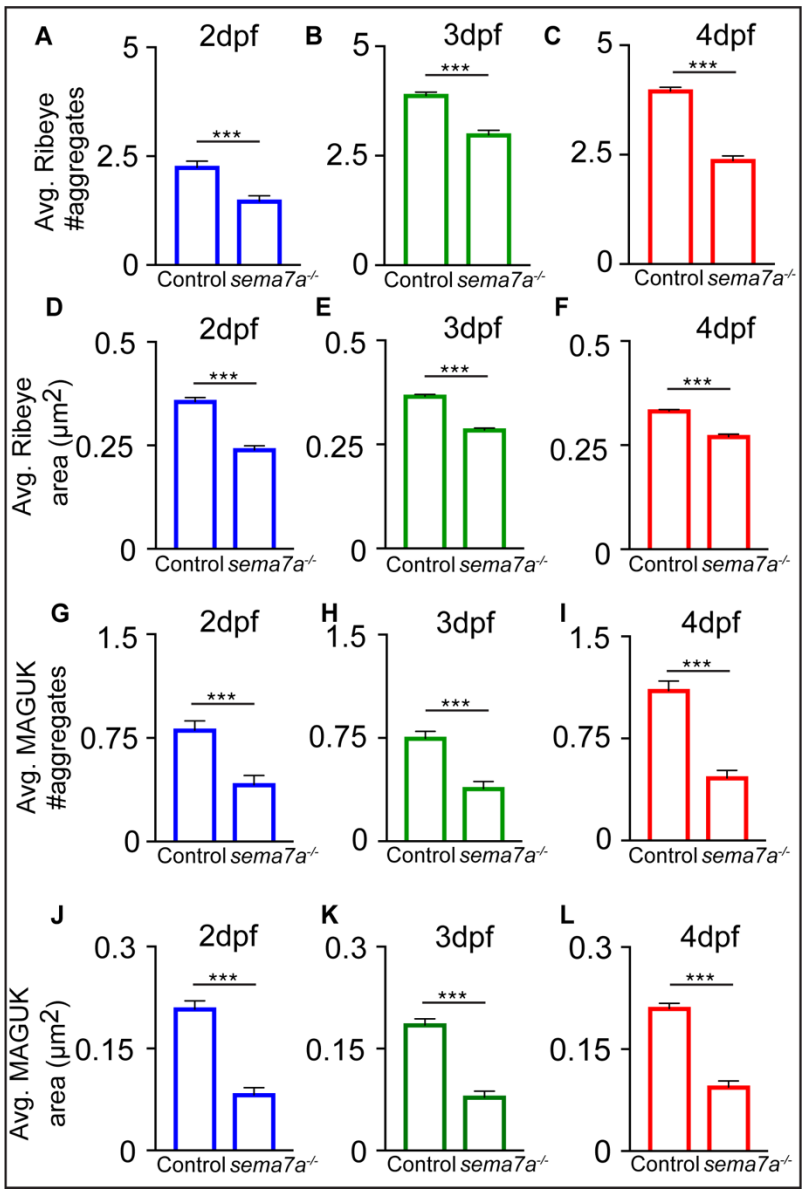

624

625 **Supplementary Figure 4. *sema7a*$^{-/-}$ mutants display impaired synaptic assembly.**
626 (A-F) The plots quantitate the average numbers and areas of presynaptic aggregates from
627 control and *sema7a*$^{-/-}$ neuromasts. Significant decreases in the numbers and areas of
628 presynaptic aggregates are observed across development. Three hundred and forty-one, 1229,
629 and 1286 presynaptic aggregates were analyzed from 2 dpf, 3 dpf, and 4 dpf control larvae,
630 respectively. Two hundred and thirty-five, 643, and 419 presynaptic aggregates were analyzed
631 from 2 dpf, 3 dpf, and 4 dpf *sema7a*$^{-/-}$ mutant larvae, respectively. (G-L) The plots quantitate
632 the average numbers and areas of postsynaptic aggregates from control and *sema7a*$^{-/-}$
633 neuromasts. Significant decreases in the numbers and areas of postsynaptic aggregates
634 occurred during development. Three hundred and ninety-seven, 1243, and 1300 postsynaptic

aggregates were analyzed from 2 dpf, 3 dpf, and 4 dpf control larvae, respectively. Three hundred and four, 651, and 451 postsynaptic aggregates were analyzed from 2 dpf, 3 dpf, and 4 dpf *sema7a*$^{-/-}$ mutant larvae, respectively. Means ± SEMs; *** implies $p < 0.001$.

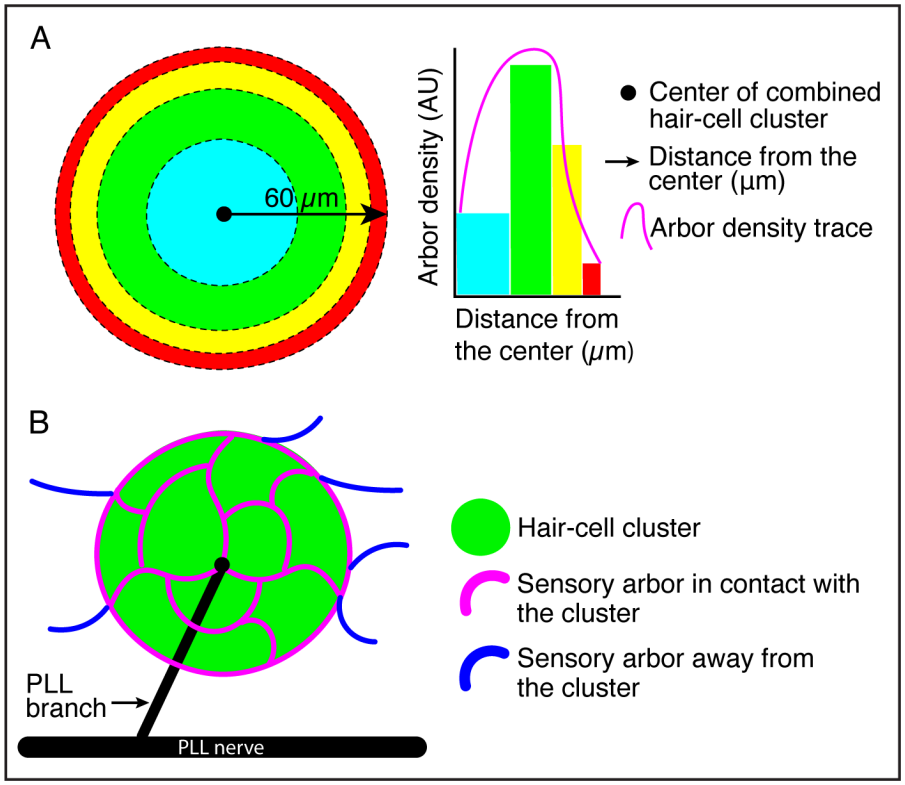

Supplementary Figure 5. Quantification of sensory arbor distributions and contacts with hair cell clusters. (A) A schematic drawing of the combined hair cell cluster and surrounding region depicts concentric sections of equal area in distinct colors (cyan, green, yellow, and blue). The arbor density is plotted as a histogram against the distance (black arrow) from the center (black circle) of the combined hair cell cluster. The histogram is represented as a density trace graph (magenta). (B) A schematic drawing of a posterior lateral line neuromast depicts the posterior lateral line (PLL) nerve (black), posterior lateral line branch (black), the sensory arbors (magenta) that contact the hair cell cluster (green), and the sensory arbors that project away (blue) from the hair cell cluster.

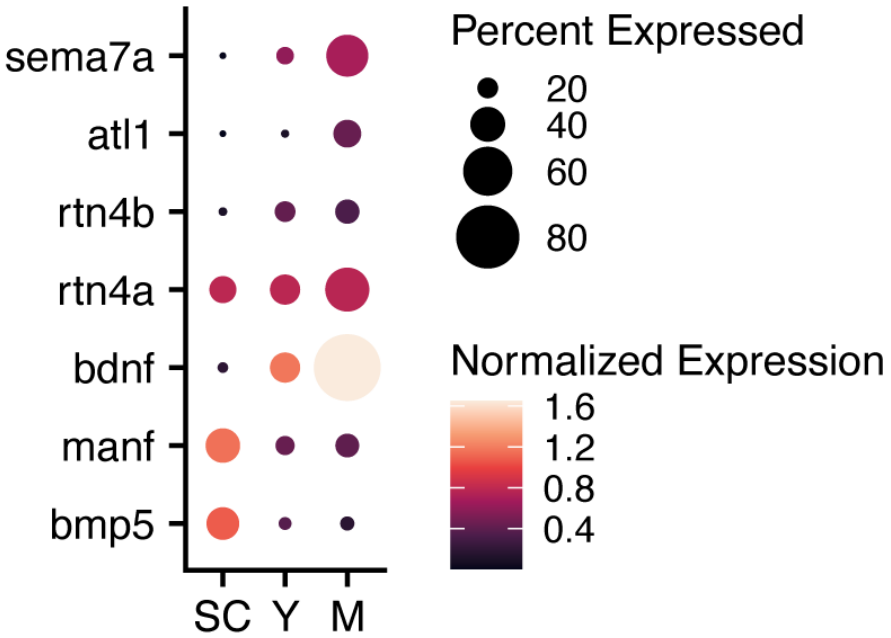

Supplementary Figure 6. Expression of diverse neural guidance cues in developing neuromasts. Analysis of single cell RNA-sequencing data (9) shows the expression of multiple neural guidance genes that are expressed across young hair cells (Y), mature hair cells (M), and support cells (SC). Dot sizes and colors signify the proportion of cells in each cluster that express a gene and the average strength of expression (ln[(counts/10,000) +1]), respectively.

664 1. Lykissas M, Batistatou A, Charalabopoulos K, Beris A. The Role of Neurotrophins in
665 Axonal Growth, Guidance, and Regeneration. Curr Neurovasc Res. 2007 May 1;4(2):143–
666 51.
667 2. Vaccaro G, Dumoulin A, Zuñiga NR, Bandtlow CE, Stoeckli ET. The Nogo-66 Receptors
668 NgR1 and NgR3 Are Required for Commissural Axon Pathfinding. J Neurosci. 2022 May
669 18;42(20):4087–100.
670 3. Nguyen-Ba-Charvet KT, Di Meglio T, Fouquet C, Chedotal A. Robos and Slits Control the
671 Pathfinding and Targeting of Mouse Olfactory Sensory Axons. J Neurosci. 2008 Apr
672 16;28(16):4244–9.
673 4. Jeroen Pasterkamp R, Peschon JJ, Spriggs MK, Kolodkin AL. Semaphorin 7A promotes
674 axon outgrowth through integrins and MAPKs. Nature. 2003 Jul;424(6947):398–405.
675 5. Nagiel A, Andor-Ardo D, Hudspeth AJ. Specificity of Afferent Synapses onto Plane-
676 Polarized Hair Cells in the Posterior Lateral Line of the Zebrafish. J Neurosci. 2008 Aug
677 20;28(34):8442–53.
678 6. Jacobo A, Dasgupta A, Erzberger A, Siletti K, Hudspeth AJ. Notch-Mediated
679 Determination of Hair-Bundle Polarity in Mechanosensory Hair Cells of the Zebrafish
680 Lateral Line. Curr Biol. 2019 Nov;29(21):3579-3587.e7.
681 7. Valera G, Markov DA, Bijari K, Randlett O, Asgharsharghi A, Baudoin JP, et al. A
682 neuronal blueprint for directional mechanosensation in larval zebrafish. Curr Biol. 2021
683 Apr;31(7):1463-1475.e6.
684 8. Dow E, Jacobo A, Hossain S, Siletti K, Hudspeth AJ. Connectomics of the zebrafish's
685 lateral-line neuromast reveals wiring and miswiring in a simple microcircuit. eLife. 2018
686 Jun 12;7:e33988.
687 9. Lush ME, Diaz DC, Koenecke N, Baek S, Boldt H, St Peter MK, et al. scRNA-Seq reveals
688 distinct stem cell populations that drive hair cell regeneration after loss of Fgf and Notch
689 signaling. eLife. 2019 Jan 25;8:e44431.
690 10. Carulli D, de Winter F, Verhaagen J. Semaphorins in Adult Nervous System Plasticity and
691 Disease. Front Synaptic Neurosci. 2021 May 11;13:672891.

692 11. Yazdani U, Terman JR. The semaphorins. Genome Biol. 2006;7(3):211.
693 12. de Winter F, Kwok JCF, Fawcett JW, Vo TT, Carulli D, Verhaagen J. The Chemorepulsive
694 Protein Semaphorin 3A and Perineuronal Net-Mediated Plasticity. Neural Plast.
695 2016;2016:1–14.
696 13. Coate TM, Spita NA, Zhang KD, Isgrig KT, Kelley MW. Neuropilin-2/Semaphorin-3F-
697 mediated repulsion promotes inner hair cell innervation by spiral ganglion neurons. eLife.
698 2015 Aug 24;4:e07830.
699 14. Carcea I, Patil SB, Robison AJ, Mesias R, Huntsman MM, Froemke RC, et al. Maturation
700 of cortical circuits requires Semaphorin 7A. Proc Natl Acad Sci. 2014 Sep
701 23;111(38):13978–83.
702 15. Inoue N, Nishizumi H, Naritsuka H, Kiyonari H, Sakano H. Sema7A/PlxnCl signaling
703 triggers activity-dependent olfactory synapse formation. Nat Commun. 2018
704 Dec;9(1):1842.
705 16. Inoue N, Nishizumi H, Ooyama R, Mogi K, Nishimori K, Kikusui T, et al. The olfactory
706 critical period is determined by activity-dependent Sema7A/PlxnC1 signaling within
707 glomeruli. eLife. 2021 Mar 29;10:e65078.
708 17. Morote-Garcia JC, Napiwotzky D, Köhler D, Rosenberger P. Endothelial Semaphorin 7A
709 promotes neutrophil migration during hypoxia. Proc Natl Acad Sci. 2012 Aug
710 28;109(35):14146–51.
711 18. Nishide M, Kumanogoh A. The role of semaphorins in immune responses and
712 autoimmune rheumatic diseases. Nat Rev Rheumatol. 2018 Jan;14(1):19–31.
713 19. Köhler D, Granja T, Volz J, Koeppen M, Langer HF, Hansmann G, et al. Red blood cell-
714 derived semaphorin 7A promotes thrombo-inflammation in myocardial ischemia-
715 reperfusion injury through platelet GPIb. Nat Commun. 2020 Dec;11(1):1315.
716 20. Pham TL, He J, Kakazu AH, Jun B, Bazan NG, Bazan HEP. Defining a mechanistic link
717 between pigment epithelium–derived factor, docosahexaenoic acid, and corneal nerve
718 regeneration. J Biol Chem. 2017 Nov;292(45):18486–99.
719 21. Xie J, Wang H. Semaphorin 7A as a potential immune regulator and promising

720 therapeutic target in rheumatoid arthritis. Arthritis Res Ther. 2017 Dec;19(1):10.
721 22. Dow E, Siletti K, Hudspeth AJ. Cellular projections from sensory hair cells form polarity-
722 specific scaffolds during synaptogenesis. Genes Dev. 2015 May 15;29(10):1087–94.
723 23. Pujol-Martí J, Faucherre A, Aziz-Bose R, Asgharsharghi A, Colombelli J, Trapani JG, et
724 al. Converging Axons Collectively Initiate and Maintain Synaptic Selectivity in a Constantly
725 Remodeling Sensory Organ. Curr Biol. 2014 Dec;24(24):2968–74.
726 24. De Wit J, De Winter F, Klooster J, Verhaagen J. Semaphorin 3A displays a punctate
727 distribution on the surface of neuronal cells and interacts with proteoglycans in the
728 extracellular matrix. Mol Cell Neurosci. 2005 May;29(1):40–55.
729 25. Sharma P, Ruel TD, Kocha KM, Liao S, Huang P. Single cell dynamics of embryonic
730 muscle progenitor cells in zebrafish. Development. 2019 Jan 1;dev.178400.
731 26. Keenan SR, Currie PD. The Developmental Phases of Zebrafish Myogenesis. J Dev Biol.
732 2019 Jun 2;7(2):12.
733 27. Sato A, Koshida S, Takeda H. Single-cell analysis of somatotopic map formation in the
734 zebrafish lateral line system. Dev Dyn. 2010 Jul;239(7):2058–65.
735 28. Shen K, Cowan CW. Guidance Molecules in Synapse Formation and Plasticity. Cold
736 Spring Harb Perspect Biol. 2010 Apr 1;2(4):a001842–a001842.
737 29. Um JW, Ko J. Neural Glycosylphosphatidylinositol-Anchored Proteins in Synaptic
738 Specification. Trends Cell Biol. 2017 Dec;27(12):931–45.
739 30. Uesaka N, Uchigashima M, Mikuni T, Nakazawa T, Nakao H, Hirai H, et al. Retrograde
740 semaphorin signaling regulates synapse elimination in the developing mouse brain.
741 Science. 2014 May 30;344(6187):1020–3.
742 31. Sheets L, Hagen MW, Nicolson T. Characterization of Ribeye Subunits in Zebrafish Hair
743 Cells Reveals That Exogenous Ribeye B-Domain and CtBP1 Localize to the Basal Ends
744 of Synaptic Ribbons. Riley B, editor. PLoS ONE. 2014 Sep 10;9(9):e107256.
745 32. Oliva C, Escobedo P, Astorga C, Molina C, Sierralta J. Role of the maguk protein family in
746 synapse formation and function. Dev Neurobiol. 2012 Jan;72(1):57–72.
747 33. Suli A, Pujol R, Cunningham DE, Hailey DW, Prendergast A, Rubel EW, et al. Innervation

748 regulates synaptic ribbons in lateral line mechanosensory hair cells. J Cell Sci. 2016 Jan
749 1;jcs.182592.
750 34. Taschenberger H, Leão RM, Rowland KC, Spirou GA, von Gersdorff H. Optimizing
751 Synaptic Architecture and Efficiency for High-Frequency Transmission. Neuron. 2002
752 Dec;36(6):1127–43.
753 35. Myers JP, Gomez TM. Focal Adhesion Kinase Promotes Integrin Adhesion Dynamics
754 Necessary for Chemotropic Turning of Nerve Growth Cones. J Neurosci. 2011 Sep
755 21;31(38):13585–95.
756 36. O'Donnell M, Chance RK, Bashaw GJ. Axon Growth and Guidance: Receptor Regulation
757 and Signal Transduction. Annu Rev Neurosci. 2009 Jun 1;32(1):383–412.
758 37. Gilmour D, Knaut H, Maischein HM, Nüsslein-Volhard C. Towing of sensory axons by
759 their migrating target cells in vivo. Nat Neurosci. 2004 May;7(5):491–2.
760 38. Metcalfe WK. Sensory neuron growth cones comigrate with posterior lateral line
761 primordial cells in zebrafish. J Comp Neurol. 1985 Aug 8;238(2):218–24.
762 39. Gasanov EV, Rafieva LM, Korzh VP. BDNF-TrkB Axis Regulates Migration of the Lateral
763 Line Primordium and Modulates the Maintenance of Mechanoreceptor Progenitors. Proost
764 P, editor. PLOS ONE. 2015 Mar 9;10(3):e0119711.
765 40. Schuster K, Dambly-Chaudière C, Ghysen A. Glial cell line-derived neurotrophic factor
766 defines the path of developing and regenerating axons in the lateral line system of
767 zebrafish. Proc Natl Acad Sci. 2010 Nov 9;107(45):19531–6.
768 41. Germanà A, Laurà R, Montalbano G, Guerrera MC, Amato V, Zichichi R, et al. Expression
769 of Brain-Derived Neurotrophic Factor and TrkB in the Lateral Line System of Zebrafish
770 During Development. Cell Mol Neurobiol. 2010 Jul;30(5):787–93.
771 42. Ji YR, Warrier S, Jiang T, Wu DK, Kindt KS. Directional selectivity of afferent neurons in
772 zebrafish neuromasts is regulated by Emx2 in presynaptic hair cells. eLife. 2018 Apr
773 19;7:e35796.
774 43. Kindt KS, Finch G, Nicolson T. Kinocilia Mediate Mechanosensitivity in Developing
775 Zebrafish Hair Cells. Dev Cell. 2012 Aug;23(2):329–41.

776 44. Obholzer N, Wolfson S, Trapani JG, Mo W, Nechiporuk A, Busch-Nentwich E, et al.
777 Vesicular Glutamate Transporter 3 Is Required for Synaptic Transmission in Zebrafish
778 Hair Cells. J Neurosci. 2008 Feb 27;28(9):2110–8.
779 45. Kwan KM, Fujimoto E, Grabher C, Mangum BD, Hardy ME, Campbell DS, et al. The
780 Tol2kit: A multisite gateway-based construction kit forTol2 transposon transgenesis
781 constructs. Dev Dyn. 2007 Nov;236(11):3088–99.
782 46. Arshadi C, Günther U, Eddison M, Harrington KIS, Ferreira TA. SNT: a unifying toolbox
783 for quantification of neuronal anatomy. Nat Methods. 2021 Apr;18(4):374–7.